DOI:
10.1021/acs.bioconjchem.0c00401

Document Version
Peer reviewed version

[^{68}Ga]Ga-THP-Pam: A Bisphosphonate PET tracer with Facile Radiolabelling and Broad Calcium Mineral Affinity

George P. Keeling,[a] Billie Sherin,[a] Jana Kim,[a] Belinda San Juan,[a] Tilmann Grus,[b] Thomas R. Eykyn,[a] Frank Rösch,[b] Gareth Smith,[c] Philip J. Blower,[a] Samantha Y. A. Terry,[a] and Rafael T. M. de Rosales[a*]

[a] School of Biomedical Engineering & Imaging Sciences, King's College London, St Thomas' Hospital, London, SE1 7EH, U.K.

[b] Department of Nuclear Chemistry, Johannes Gutenberg University Mainz, Fritz-Strassmann-Weg 2, D-55128 Mainz, Germany.

[c] Theragnostics Ltd, 2 Arlington Square, Bracknell, Berkshire, RG12 1WA, U.K.

*E-mail: rafael.torres@kcl.ac.uk

Abstract

Calcium minerals such as hydroxyapatite (HAp) can be detected non-invasively *in vivo* using nuclear imaging agents such as [^{18}F]NaF (available from cyclotrons), for positron emission tomography (PET) and ^{99m}Tc-radiolabelled bisphosphonates (BP; available from ^{99m}Tc generators for single photon emission computed tomography (SPECT) or scintigraphy). These two types of imaging agents allow detection of bone metastases (based on the presence of HAp) and vascular calcification lesions (that contain HAp and other calcium minerals). With the aim of developing a cyclotron-independent PET radiotracer for these lesions, with broad calcium mineral affinity and simple one-step radiolabelling, we developed [^{68}Ga]Ga-THP-Pam. Radiolabelling with ^{68}Ga is achieved using a mild single-step kit (5 min, room temperature, pH 7) to high radiochemical yield and purity (>95%). NMR studies demonstrate that Ga binds *via* the THP chelator, leaving the BP free to bind to its biological target. [^{68}Ga]Ga-THP-Pam shows high stability in human serum. The calcium mineral binding of [^{68}Ga]Ga-THP-Pam was compared *in vitro* to two other ^{68}Ga-BPs which have been successfully evaluated in humans, [^{68}Ga]Ga-NO2AP^{BP} and [^{68}Ga]Ga-BPAMD, as well as [^{18}F]NaF. Interestingly, we found that all ^{68}Ga-BPs have a high affinity for a broad range of calcium minerals implicated in vascular calcification disease, while [^{18}F]NaF is selective for HAp. Using healthy young mice as a model of metabolically active growing calcium mineral *in vivo*, we compared the pharmacokinetics and biodistribution of [^{68}Ga]Ga-THP-Pam with [^{18}F]NaF as well as [^{68}Ga]NO2AP^{BP}. These studies revealed that [^{68}Ga]Ga-THP-Pam has high *in vivo* affinity for bone tissue (high bone/muscle and bone/blood ratios) and fast blood clearance ($t_{1/2}$ <10 min) comparable to both [^{68}Ga]NO2AP^{BP} and [^{18}F]NaF. Overall, [^{68}Ga]Ga-THP-Pam shows high potential for clinical translation as a cyclotron-independent calcium mineral PET radiotracer, with simple and efficient radiochemistry that can be easily implemented in any radiopharmacy.

Introduction

Calcium is an essential element in human biology and the most abundant metallic element in the body by weight.[1,2] The majority of body calcium is in the form of a solid mineral, hydroxyapatite (HAp; $Ca_5(PO_4)_3(OH)$) in bones.[3] This calcium mineral can be targeted *in vivo* using bisphosphonates (BPs, Scheme 1A), which led to the development of BP-based radiotracers such as [^{99m}Tc]Tc-methylene diphosphonate (MDP) (^{99m}Tc; $t_{1/2}$ = 6.02 h). Introduced half a century ago, [^{99m}Tc]Tc-MDP is still widely used in nuclear medicine to image bone disease, particularly metastatic cancer in the bones using single photon emission computed tomography (SPECT) imaging (Scheme 1A).[4-7] Its chemical structure, however, remains unknown.[8]

In recent years there has been increasing interest in performing bone scans using positron emission tomography (PET) imaging. This is due to its better sensitivity and spatial resolution, compared to SPECT, which allows the detection of smaller lesions as well as improved image quantification. The radiotracer of choice in clinical PET imaging of bone lesions is the sodium salt of [^{18}F]fluoride (^{18}F; $t_{1/2}$ = 110 min; β^+ = 97%).[9-11] Interestingly, [^{18}F]NaF binds HAp not by interacting with calcium but by displacement of the hydroxide in the HAp lattice (Scheme 1A).[12]

A

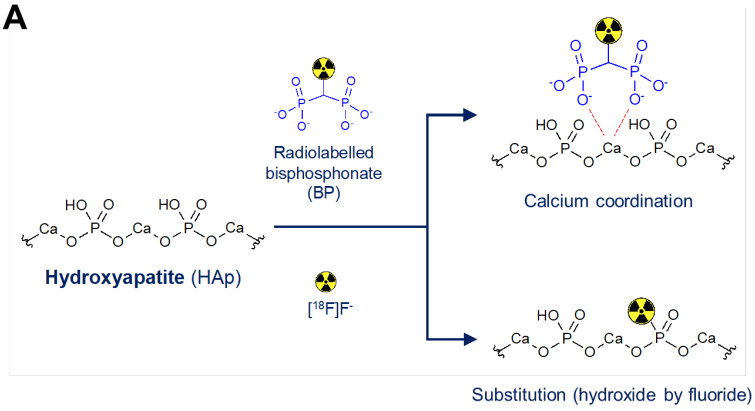

B

Calcium salt	Formula
Hydroxyapatite	$Ca_5(PO_4)_3(OH)$
Calcium oxalate	$C_2O_4Ca{\cdot}H_2O$
β-tricalcium phosphate	$Ca_3(PO_4)_2$
Whitlockite	$(Ca,Mg)_3(PO_4)_2$
Calcium carbonate	$CaCO_3$
Calcium pyrophosphate	$Ca_2P_2O_7$
Amorphous calcium phosphate	$Ca_3(PO_4)_2{\cdot}xH_2O$

Scheme 1. (A) Schematic showing the proposed binding of bisphosphonate (BP)-based imaging agents and [^{18}F]NaF to hydroxyapatite (HAp); (B) Formulae of the different calcium salts discussed in this work.

Besides HAp, other calcium minerals are implicated in a number of health conditions in which a sensitive, non-invasive imaging method such as PET would be of great use. One

such example is vascular calcification, a clinical marker of atherosclerosis in which soft vascular tissue forms plaques that can occlude the flow of blood through the affected vessel and can rupture, causing potentially fatal downstream effects.[13] Atherosclerosis can lead to cardiovascular disease (CVD), the leading cause of death globally with *ca*. 18 million deaths in 2016 and an upward trend expected over the next decade.[14] The primary composition of vascular calcification lesions is disputed in the literature, with not only HAp, but also calcium oxalate monohydrate, and β-tricalcium phosphate partially substituted with magnesium (whitlockite) being reported as the main components.[15-20] Other calcium minerals such as calcium carbonate, calcium pyrophosphate and amorphous calcium phosphate have also been reported, as well as heterogeneous composition between patients.[15,18,21] Thus, it seems that calcium in these lesions is present as a mixture that may contain several non-HAp materials, summarised in Scheme 1B. The role that these non-HAp calcium minerals may have in different stages of CVD, and their potential as imaging biomarkers, remain to be elucidated.

Despite the advantages of [^{18}F]NaF as a PET radiotracer, its binding mechanism and *in vitro/vivo* data indicate that its target *in vivo* is HAp (Scheme 1A) and not other calcium minerals that have also been identified in vascular calcification lesions.[22,23] BPs on the other hand are not selective for HAp, showing broader calcium mineral affinity.[24,25] Hence, there is considerable interest in the development of BP-based PET radiotracers. These should allow the detection of bone lesions, as recently demonstrated in patients,[5,26-30] but also calcified vasculature which we have discussed above may contain different types of calcium minerals besides HAp and thus may benefit from the broader calcium mineral affinity of BPs.

From the radiopharmacy and clinical translation perspective, a disadvantage of current BP-based PET radiotracers is a relatively complex radiochemistry. ^{18}F is produced by cyclotrons, which are expensive and complex instruments, but can produce [^{18}F]NaF in large quantities without any further need for complicated radiosynthetic procedures.[10] On the other hand, PET BPs rely on the use of radiometals and hence are bifunctional chelators that generally involve multi-step syntheses and radiosynthetic procedures, which may require an automated synthesis module for clinical translation.[5,26-28,31-40] The most promising radionuclide in the development of PET BPs is ^{68}Ga ($t_{1/2}$ = 68 min; β^+ = 89%). This radiometal not only benefits from a short radiation decay half-life that minimises radiation dose to patients, but also availability from both cyclotrons and benchtop generators that can be installed in any radiopharmacy, allowing cyclotron-independent PET radiotracers on-site.[41] Having a variety

of such cyclotron-independent radiotracers is attractive as it would not only provide an alternative supply of some PET radiotracers in case of cyclotron failures, but also potentially open the door to cyclotron-independent PET scanners, widening access to PET for patients geographically distant from cyclotron centres. Notable examples of ^{68}Ga radiotracers that are increasingly being exploited for clinical PET today include those based on PSMA for imaging prostate cancer,[42-44] octreotide analogues for neuroendocrine tumours,[45] and recently FAP inhibitors, which shows exciting prospects as a pan-cancer PET imaging agent.[46]

We set out to create a BP-based "cold kit" radiopharmaceutical for PET imaging of calcium minerals, in which ^{68}Ga generator eluate could be added directly to a vial containing pre-formulated reagents and used without any further steps. Our motivation was not only to explore the broad calcium mineral affinity of BPs, but also to combine the superior performance of PET imaging with the simplicity of radionuclide generator kit-based synthesis and availability, that has been largely responsible for the long-term success of ^{99m}Tc radiochemistry and the nuclear imaging field. Here, we describe the development of [^{68}Ga]Ga-THP-Pam, a ^{68}Ga complex of the efficient gallium chelator (*tris*)hydroxypyridinone (THP),[44, 47-57] conjugated with the clinically used BP pamidronate (Pam) (Figure 1A) and its comparison with [^{18}F]NaF and two other ^{68}Ga-labelled BPs—BPAMD (Figure 1B) and NO2AP^{BP} (Figure 1C)—which have undergone extensive evaluation including first in human studies.[5, 26-28, 31-33, 58]

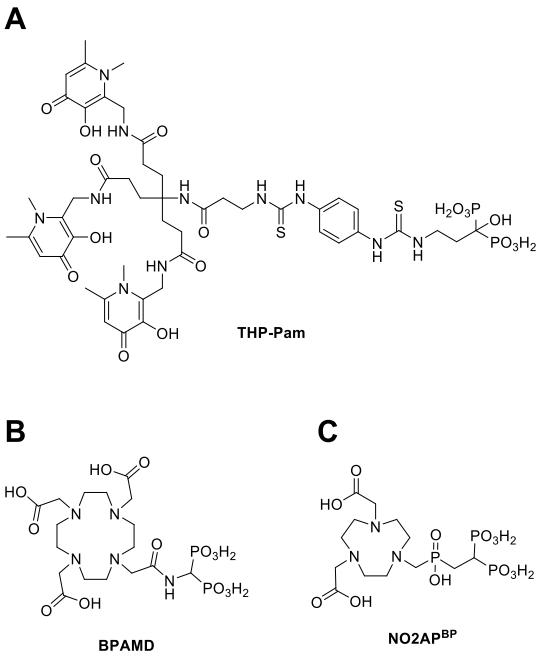

Figure 1. Chemical structures of the bifunctional bisphosphonate chelators discussed in this work. (A) THP-Pam; (B) BPAMD; (C) NO2AP^{BP}.

Results and discussion

Synthesis of THP-Pam. The bifunctional chelator THP-Pam was designed to include a (*tris*)hydroxypyridinone group for efficient gallium chelation, as well as the bone-targeting moiety pamidronate (Pam), a clinically-used aminobisphosphonate with known high affinity for bone mineral.[59] Pamidronate was synthesised according to a literature procedure (Scheme 2A),[60] leading to a pure white solid with a shelf-life at room temperature of at least 4485 days, as measured by NMR, MS and elemental analysis. Among the clinically used second generation amino-BPs, pamidronate has the shorter chain between the BP and the amine groups, keeping the overall size of the molecule as small as possible, which generally leads to faster pharmacokinetics (PK).

In order to form the conjugate, the primary amine group of pamidronate was reacted with THP-isothiocyanate[50] in a single step (Scheme 2B). Water was chosen as the solvent for this reaction due to the poor solubility of amino-BPs in organic solvents.[24] This however opened the possibility of the slow degradation of the isothiocyanate in water. To increase the speed of reaction and reduce the likelihood of degradation, a minimal volume of solvent was used and the reaction was performed at 90°C in a sealed vial with a large excess of pamidronate to help drive the desired reaction. Triethylamine was used to achieve a reaction pH of ~11 in order to deprotonate the amine of pamidronate (pK_a = 10.40–13.06),[61] and allow the reaction to proceed. The high pH increased the water solubility of both pamidronate and THP-NCS. Monitoring the progress of the reaction by LC/MS indicated that 2 h was the optimal reaction time. These reaction conditions were successful in reducing the number of by-products; the only products observed by LC/MS, aside from excess pamidronate, were >90% THP-Pam (*m/z* $[M + 2H]^{2+}$ = 598) and <10 % THP-NCS hydrolysed to a primary amine (*m/z* $[M + 2H]^{2+}$ = 460).

The resulting thiourea bond has been reported to be less stable than amide bonds,[62,63] however thiourea bonds have also been shown to be stable *in vivo* over timescales of up to 24 h.[64] Due to the short circulation time of BPs and short half-life of ^{68}Ga, the risk of hydrolysis of the thiourea bond during imaging was considered to be minimal. An amide bond formation would have been an alternative bioconjugation strategy, using *N*-hydroxysuccinimide esters. However, the relatively fast hydrolysis of the activated esters would have made water an unsuitable solvent for the required bioconjugation conditions (high pH and T) and the

commercial availability of THP-isothiocyanate allowed for a more straightforward synthetic approach.

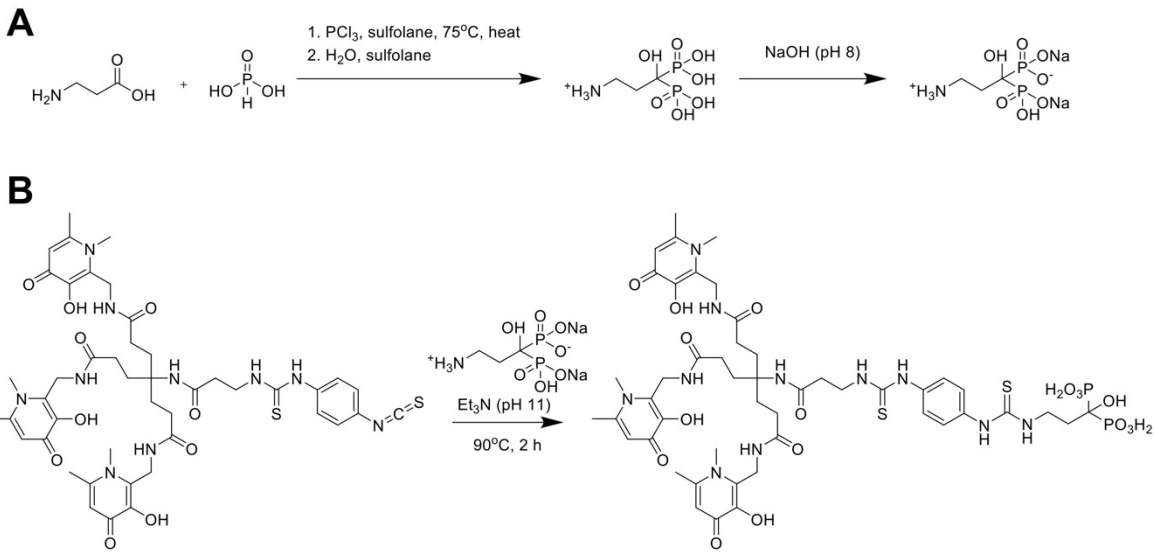

Scheme 2. Synthesis of THP-Pam. (A) Synthesis of the amino-BP pamidronate; (B) Thiourea bond formation between pamidronate and THP-NCS yields THP-Pam in 71% yield.

To remove the unreacted pamidronate, the reaction solution was loaded onto a Sep-Pak tC18 cartridge, from which pamidronate could selectively be eluted in water (0.1% TFA), while the other products were subsequently eluted in 1:1 water:acetonitrile (0.1% TFA). Collecting small volume fractions, those with the most THP-Pam and least hydrolysed THP-NCS, as measured using LC/MS, were collected. LC/MS analysis of the collated fractions confirmed the success of this purification step, with a final purity of >95% THP-Pam. After evaporation, THP-Pam was obtained as a white powder in 71% yield and no further attempts were made to optimise reaction conditions. The product can also be purified by semi-preparative HPLC (HPLC method 1 (Table S1); t_R = 20.9 min).

Characterisation of THP-Pam. Analytical C_{18} reverse-phase HPLC analysis showed a single peak (Figure 2A) with some tailing, indicating a pure product with multiple ionisation states or different modes of retention on the stationary phase, as previously seen for other BP compounds.[24,31,32,38] THP-Pam eluted at t_R =10.4 minutes (HPLC method 2 (Table S2)), at which point the mobile phase is ~70% water, as confirmed by LC/MS analysis (Figure 2B). Pamidronate, on the other hand, elutes at t_R = 1.7 minutes under the same conditions. After purification, LC/MS analyses occasionally indicated the presence of THP-Pam + Fe (*m/z* $[M + 2H]^{2+}$ = 625). This highlights the tendency for both THP and BPs to bind to metals ions,

especially iron(III),[54,65-67] and the importance of avoiding metal contamination at any stage of reaction. Upon binding to iron, THP-Pam changes from a white powder to a pink or red powder, providing an extremely sensitive indicator of the presence of iron.[55] As this was not the case with our purified product, it was assumed that the iron was bound during transition through the LC/MS system and was not present in the product.

The $^{31}P\{^{1}H\}$ NMR spectrum of THP-Pam showed a single peak at 17.86 ppm, and consistent with the chemical shift for a BP (Figure 2C). The ^{1}H NMR spectrum also showed the expected resonances for THP-Pam, however all peaks were rather broad (Figure 2D). This is likely due to different ionisation states of the molecule causing different conformations or small degrees of iron binding from solvent impurities. ^{19}F NMR revealed the presence of TFA salts in the final product (Figure 2E), even after low-vacuum evaporation. This was further confirmed by elemental analysis and is due to the presence of TFA in the mobile phases used during purification of THP-Pam.

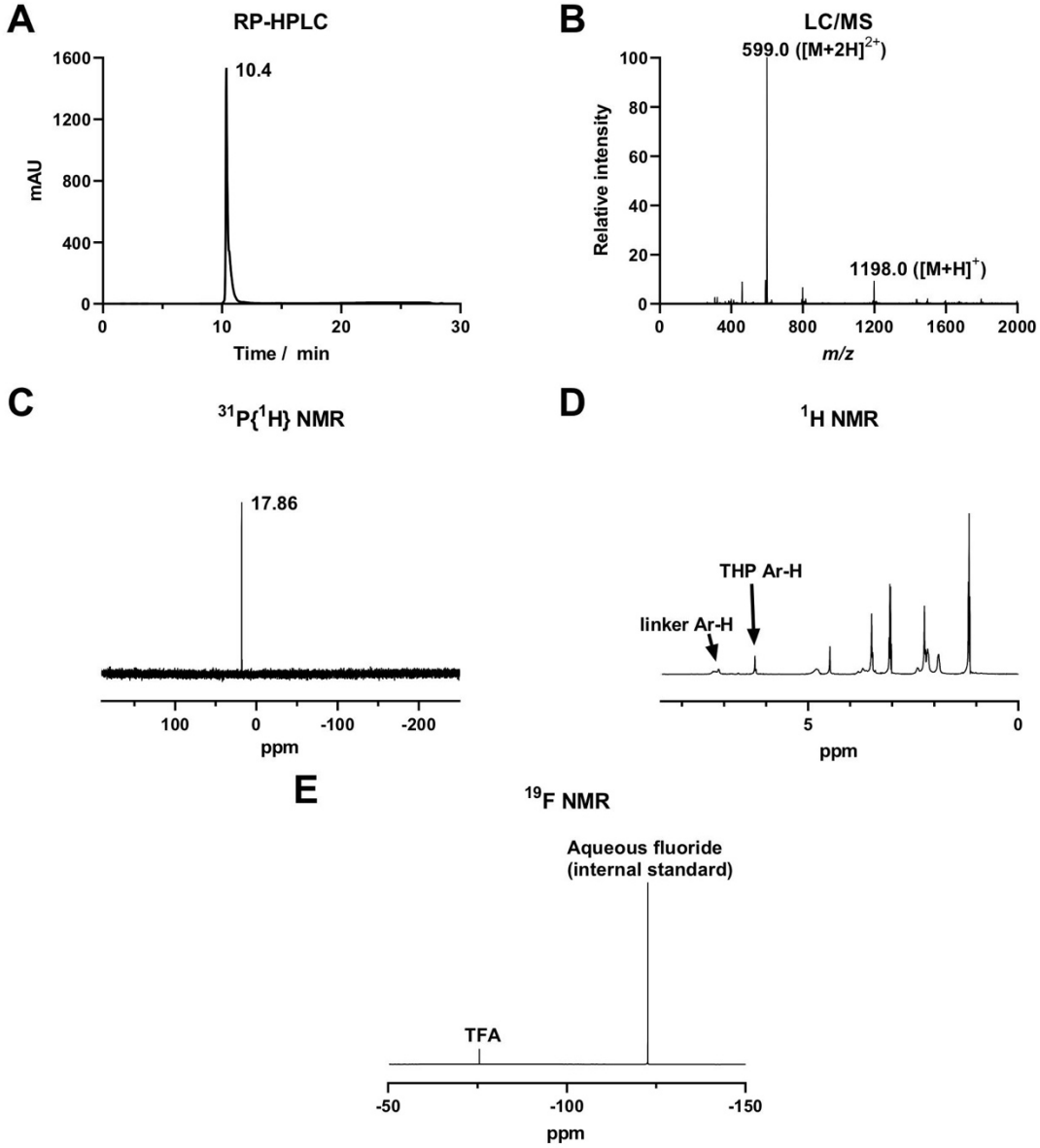

Figure 2. Characterisation of THP-Pam. (A) Reverse-phase C_{18} HPLC UV (254 nm); (B) ESI-MS spectrum (+ve mode) from LC/MS; (C) $^{31}P\{^{1}H\}$ NMR in D_2O; (D) ^{1}H NMR in D_2O; (E) ^{19}F NMR in D_2O confirming the presence of TFA salts.

As both pamidronate and THP are known metal chelators,[49,68] we conducted NMR studies in order to determine whether gallium will preferentially bind to THP, as expected due to its high affinity towards this metal, or if the BP could be involved. This is an important factor as competing of the BP with the chelator for the binding of gallium-68 has been noted in previous BP-based tracers.[32,36] To investigate this possibility, an aqueous solution (D_2O) of THP-Pam of known concentration and adjusted to pH 9 by addition of Na_2CO_3 was prepared at room temperature. To this solution, known amounts of non-radioactive gallium nitrate were

added incrementally and the binding process monitored by $^{31}P\{^{1}H\}$ NMR to monitor the BP moiety, and the aromatic region of the ^{1}H NMR spectrum to monitor the hydroxypyridinone moieties responsible for the chelating properties of THP (Figure 3). As Ga(III) ions were added, a loss of symmetry and a change in chemical shift was observed in the aromatic region of the ^{1}H NMR spectrum (Figure 3A), indicating a change in the chemical environment of the hydroxypyridinone arms of THP and hence supportive of direct metal binding, as seen in previous THP studies.[69] Meanwhile the bisphosphonate peak in the $^{31}P\{^{1}H\}$ NMR spectrum (Figure 3B) did not change, apart from minor peak broadening likely caused by slowing of the movement of the THP arms in response to metal binding, and a minor chemical shift from 17.90 to 17.97 ppm as gallium was added. As a control, gallium nitrate was added to a solution of pamidronate under the same conditions and monitored by $^{31}P\{^{1}H\}$ NMR and, as expected, a distinct loss of symmetry and homogeneity was observed upon addition of gallium to the solution, with several new species with chemical shifts in the range of 22.4–3.0 ppm being formed (Figure 3C). Altogether, these data indicate that THP-Pam—at equimolar and sub-equimolar concentrations of gallium—will bind gallium in the THP chelator, and not the BP.

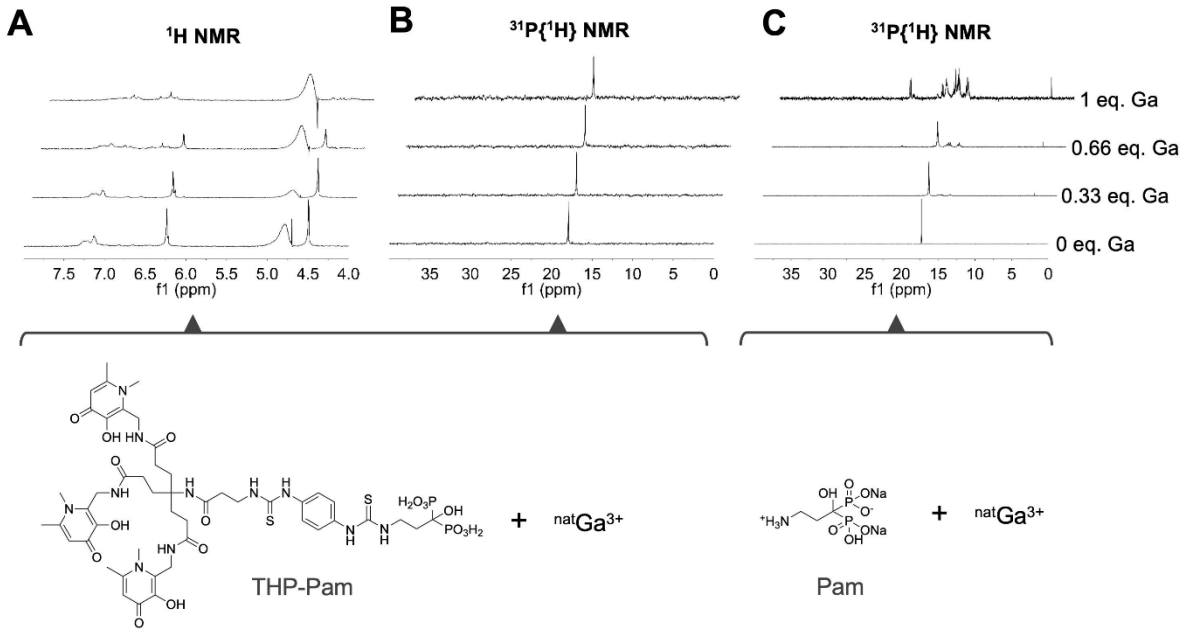

Figure 3. NMR titration experiments (D_2O and pH 9) of THP-Pam and pamidronate upon [^{nat}Ga]gallium nitrate addition demonstrating the lack of involvement of the bisphosphonate of THP-Pam in gallium binding. Each spectrum is scaled according to the largest peak shown for the sake of clarity. (A) ^{1}H NMR 4.0–7.8 ppm window showing aromatic protons of THP-Pam corresponding to hydroxypyridinone arms, which show changes in chemical shift and loss of symmetry upon gallium binding, indicating a change in chemical environment; (B) $^{31}P\{^{1}H\}$ NMR showing that BP phosphorus atoms exhibit no chemical shift or loss of symmetry or homogeneity upon gallium binding, consistent with lack of involvement; (C) $^{31}P\{^{1}H\}$ NMR showing pamidronate binding to gallium for comparative purposes, which shows a clear loss of symmetry and homogeneity upon gallium binding.

Radiochemistry. Having established that when reacting THP-Pam with gallium the metal ion binds to the THP chelator, and not the BP group, the radiolabelling reaction with ^{68}Ga was evaluated. It was found that ^{68}Ga radiolabelling is fast and efficient. In a typical reaction, a 250 μL aliquot of gallium-68 eluted from an Eckert and Ziegler ^{68}Ge/^{68}Ga generator in 0.1 M HCl was added to 4.18 nmol THP-Pam in water (5 μg) and neutralised with an aqueous 1 M solution of sodium bicarbonate. Both stock solutions were prepared using Chelex-treated water to minimise the presence of iron(III). After incubating the reaction for 5 min at room temperature, radio-ITLC and radio-HPLC indicated quantitative (>97%) complexation of ^{68}Ga (*vide infra*, Figure 4). We measured non-optimised molar activities up to 17.3 MBq nmol^{-1}. In order to simplify this further to a pre-prepared kit, it is possible to freeze-dry the THP-Pam and sodium bicarbonate prior to reaction and elute the generator directly into a vial containing the dried reactants, scaling quantities as required. This opens up the possibility of GMP kit-based production of THP-Pam by simple addition of ^{68}Ga generator eluate into a sealed vial.

Radio-ITLC was performed using glass microfibre chromatography paper (ITLC) impregnated with silicic acid in order to retain [^{68}Ga]Ga-THP-Pam as well as possible. By developing the ITLC paper in 0.5 M citrate buffer, unbound ^{68}Ga moved with the solvent front, giving a clear distinction between [^{68}Ga]Ga-THP-Pam on the baseline (Figure 4A). This is in contrast to unbound ^{68}Ga, which primarily moves with the solvent front (Figure 4C). Radio-HPLC (C18-RP) was performed under the same conditions as analytical HPLC (method 2 (Table S2)). [^{68}Ga]Ga-THP-Pam eluted as a single peak with a retention time that is approximately 30 seconds later compared to THP-Pam, consistent with the expectation that the binding of the metal to the hydroxyl and ketone groups of THP leads to a small increase in lipophilicity and hence a slightly longer retention on reverse-phase HPLC (Figure 4B). Figure 4C–D shows the ITLC and radio-HPLC chromatograms of neutralised [^{68}Ga]$GaCl_3$ for comparison. Measurement of logP in water/octanol (-2.69 ± 0.03) and $logD_{7.4}$ in PBS/octanol (-2.72 ± 0.07) showed that [^{68}Ga]Ga-THP-Pam was highly hydrophilic as expected for a BP, as well as existing gallium-68 labelled conjugates of THP.[44]

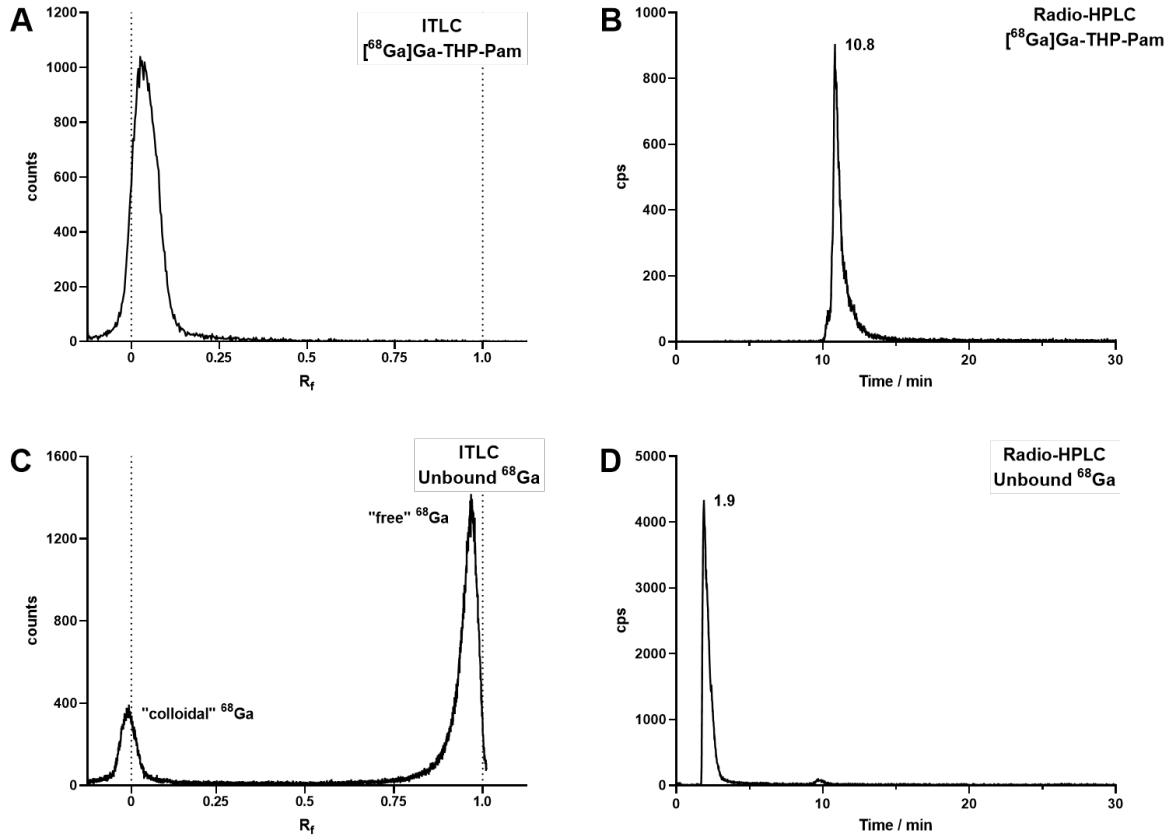

Figure 4. Radioanalysis of [^{68}Ga]Ga-THP-Pam and unbound ^{68}Ga as a comparison. (A) ITLC of [^{68}Ga]Ga-THP-Pam in 0.5 M citrate buffer pH 5.5. (B) Reverse-phase C_{18} radio-HPLC of [^{68}Ga]Ga-THP-Pam. (C) ITLC of unbound ^{68}Ga, showing migration to the solvent front other than colloidal ^{68}Ga. (D) Reverse-phase C_{18} radio-HPLC of unchelated ^{68}Ga.

The different radiochemical labelling conditions and purification steps required for the *in vivo* use of the different PET radiotracers discussed in this work (^{68}Ga-BPs and [^{18}F]NaF) have been outlined in Table 1. [^{18}F]NaF is received directly from the cyclotron and no radiochemistry is necessary, apart from two ion exchange cartridges prior to injection into patients.[10] The radiolabelling processes of [^{68}Ga]Ga-BPAMD and [^{68}Ga]NO2AP^{BP} take advantage of the well-established radiochemistry associated with their chelators. In both cases, heating to 95°C is required for radiolabelling.[31,32] Heating is a requirement for NO2AP^{BP} radiolabelling, despite the similarity between this chelator and NOTA, which can be labelled at room temperature.[70] In NO2AP^{BP}, however, the presence of the phosphonates allows the formation of an out-of-cage complex and so [^{68}Ga]Ga-NO2AP^{BP} cannot be prepared at room temperature.[32] The generator eluate may be processed prior to labelling of NO2AP^{BP} to allow milder heat to be used over a shorter time and to concentrate the eluate for greater molar activity,[71] however this increases the number of steps during the radiolabelling process.

Cooling and neutralisation of the radiolabelling reactions are also required for [^{68}Ga]Ga-NO2AP^{BP} and [^{68}Ga]Ga-BPAMD. [^{68}Ga]Ga-BPAMD also requires purification post-reaction.[31] THP-Pam on the other hand can be labelled in a single step at room temperature at neutral pH in 5 minutes. The THP chelator is selective for gallium(III) over other metals and the labelling is not affected by metallic impurities at the levels found in typical ^{68}Ge/^{68}Ga generator elutions.[54,55] The efficient labelling of THP also allows for labelling at low concentrations and obviates the need for concentration of the generator eluate prior to labelling.[49]

Table 1: Radiolabelling of the tracers evaluated in this study

Radiotracer	**Radiolabelling conditions**	**Other processing for *in vivo* use**
[^{68}Ga]Ga-THP-Pam	Radionuclide: ^{68}Ge/^{68}Ga generator Reaction conditions: 5 min, room temperature, pH 7	– None.
[^{68}Ga]Ga-BPAMD	Radionuclide: ^{68}Ge/^{68}Ga generator Reaction conditions: 15 min, 95°C, pH 4	– Post-processing of ^{68}Ge/^{68}Ga generator eluate prior to radiolabelling.* – Cooling. – Cation exchange column. – Neutralisation of reaction.
[^{68}Ga]Ga-NO2AP^{BP}	Radionuclide: ^{68}Ge/^{68}Ga generator Reaction conditions: 10 min, 95°C, pH 4	– Post-processing of ^{68}Ge/^{68}Ga generator eluate prior to radiolabelling.* – Cooling. – Neutralisation of reaction.
[^{18}F]NaF	Cyclotron production	– 2 ion exchange columns.

* Not essential; allows milder radiolabelling conditions and high molar activities

***In vitro* stability**. To evaluate the stability of [^{68}Ga]Ga-THP-Pam towards transchelation to plasma proteins, it was incubated in human serum at 37°C for 3 h and the transchelation of ^{68}Ga monitored by size-exclusion HPLC. This was monitored for 180 min, which was judged sufficient due to the short half-life of ^{68}Ga and fast pharmacokinetics commonly found with BPs (and hence imaging patients no later than 3 h post-injection). In this timeframe, no transchelation of ^{68}Ga from [^{68}Ga]Ga-THP-Pam was observed and the complex remained intact and chemically unmodified. To further evaluate the stability of [^{68}Ga]Ga-THP-Pam, it was incubated in 1 mM EDTA solution in PBS (>1000-fold excess EDTA) at 37°C for 3 h. After 3 h, the stability of [^{68}Ga]Ga-THP-Pam was

98.7 ± 1.2 %. (Figure S1). These results indicate not only the radiochemical stability of the [^{68}Ga]Ga-THP-Pam complex, but also the stability of the thiourea bonds between the chelator and the BP under these conditions.

In comparison, Fellner *et al.* reported [^{68}Ga]Ga-BPAMD showed 4.2 ± 0.8% degradation over this timescale in PBS at 37°C.[31] Serum stability has not been reported for [^{68}Ga]Ga-NO2AP^{BP}, but previous *in vivo* data both for small animals and humans demonstrated high stability for [^{68}Ga]Ga-BPAMD and [^{68}Ga]Ga-NO2AP^{BP}.[5,26-28,31-33] In support of this, the *in vivo* data reported here with [^{68}Ga]Ga-NO2AP^{BP} (*vide infra*) are in agreement with *in vivo* stability for this radiotracer.

***In vitro* calcium mineral binding.** To assess the affinity and selectivity of different ^{68}Ga-BPs and [^{18}F]NaF towards several calcium minerals that are relevant to human disease, an *in vitro* binding assay was performed. The binding of [^{68}Ga]Ga-THP-Pam, [^{68}Ga]Ga-BPAMD, [^{68}Ga]Ga-NO2AP^{BP} and [^{18}F]NaF to a range of calcium salts was compared, including blocking studies in which the calcium salts were preincubated with an excess of relevant blocking agents (non-radioactive fluoride or bisphosphonate) (Figure 5). All the tested agents showed high binding to HAp (mean binding values in the range 78–93 %) which could be blocked (mean values in the range 1–6 %). [^{68}Ga]THP-Pam exhibited specific binding to all the tested salts, with the lowest value being the binding to calcium oxalate (mean value 31%). [^{68}Ga]Ga-NO2AP^{BP} generally exhibited the highest binding across the salts tested but with different trends to [^{68}Ga]Ga-THP-Pam, showing lower binding to calcium pyrophosphate (mean binding values of 45% *vs.* 60%) but higher binding to calcium oxalate (mean binding 60%). [^{68}Ga]Ga-BPAMD generally showed the lowest binding of the ^{68}Ga-BPs, although it bound more to HAp than [^{68}Ga]Ga-THP-Pam (mean binding 87% *vs.* 78%), but lower than [^{68}Ga]Ga-NO2AP^{BP} (mean binding 93%) and showed similar calcium pyrophosphate binding (mean binding 60%) to that of [^{68}Ga]Ga-THP-Pam. Contrary to expectation, the blocking experiments of [^{18}F]NaF with calcium carbonate, calcium phosphate and calcium oxalate showed higher binding than the non-blocking experiments. The reason for this is unknown and may be due to the formation of an intermediate partially fluoridated salt due to the presence of higher concentrations of sodium fluoride in the blocking study, which can more readily bind [^{18}F]F^{-} than the original salt, although this hypothesis remains untested. Overall, it was found that ^{68}Ga-BPs and [^{18}F]NaF have high binding affinity towards HAp (mean binding of ^{68}Ga-BPs = 85.8 ± 4.3%, [^{18}F]NaF = 88.4 ± 4.6%), which could be blocked by using excess unlabelled BP or fluoride,

respectively (mean blocked binding of ^{68}Ga-BPs = 2.6 ± 1.6%, [^{18}F]NaF = 2.2 ± 0.2%). For non-HAp calcium minerals, however, only ^{68}Ga-BPs showed significant binding (mean binding of ^{68}Ga-BPs across non-HAp minerals = 51.7 ± 18.0%) whereas binding of [^{18}F]NaF was negligible (mean binding of [^{18}F]NaF across non-HAp minerals = 8.4 ± 4.6%). Thus, these results are in agreement with the binding mechanisms outlined in Scheme 1, whereby BPs are able to bind to calcium ions on the surface of all these minerals. In the case of HAp, the only mineral with available hydroxyl groups within its lattice, [^{18}F]F^- substitution results in binding to the salt.[12] This confers HAp selectivity to [^{18}F]NaF. However, affinity to other calcium minerals may be advantageous in imaging ectopic or pathological calcification as previously discussed. In this regard, BP-based tracers may be of interest, in addition to their cyclotron-independent availability, in the imaging of vascular calcification in comparison to [^{18}F]NaF. The targeting of different calcium materials may also mean that combining ^{68}Ga-BPs and [^{18}F]NaF could provide complementary information which may be diagnostically useful in identifying non-HAp calcified deposits.

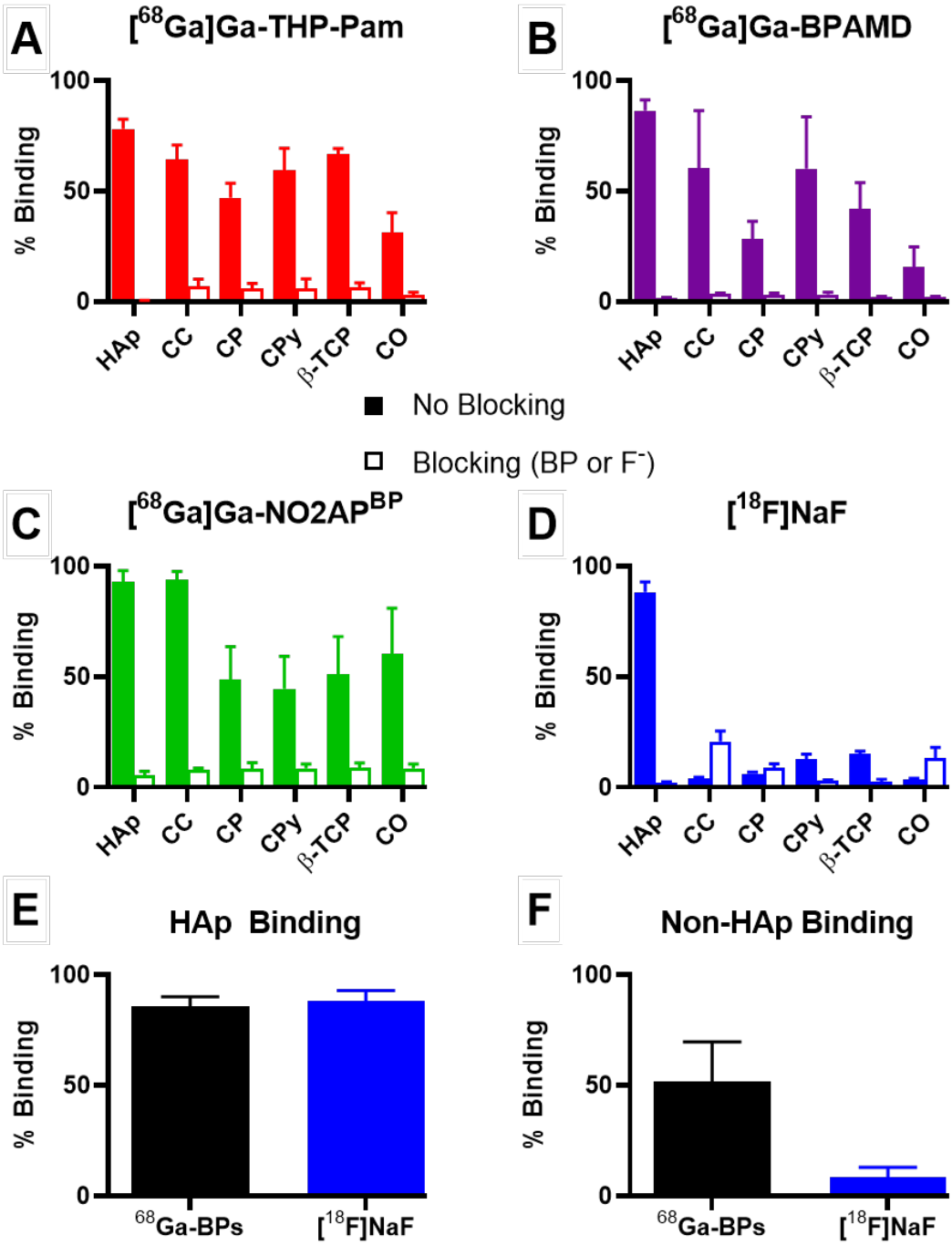

Figure 5. Binding of each radiotracer to an array of calcium salts in saline and room temperature. (A) [^{68}Ga]Ga-THP-Pam binding, blocking with pamidronate. (B) [^{68}Ga]Ga-BPAMD binding, blocking with alendronate. (C) [^{68}Ga]Ga-NO2AP^{BP} binding, blocking with pamidronate. (D) [^{18}F]NaF binding, blocking with sodium fluoride. (E) Comparison of the mean binding to HAp of ^{68}Ga-BPs and [^{18}F]NaF. (F) Comparison of the mean binding to non-HAp calcium salts of ^{68}Ga-BPs and [^{18}F]NaF. HAp = hydroxyapatite; CC = calcium carbonate; CP = calcium phosphate dibasic; CPy = calcium pyrophosphate; β-TCP = β-tricalcium phosphate; CO = calcium oxalate monohydrate.

***In vivo* evaluation**. To evaluate the *in vivo* pharmacokinetics (PK), biodistribution, and calcium mineral capabilities of these radiotracers, we compared [^{68}Ga]Ga-THP-Pam with

[^{68}Ga]NO2AP^{BP} and [^{18}F]NaF in an *in vivo* PET imaging study in 6–8 weeks old healthy immunocompetent mice. This is a good model for the *in vivo* evaluation of calcium mineral-seeking radiotracers as young mice have metabolically active growing bones. It is worth noting that [^{68}Ga]Ga-NO2AP^{BP} has previously been tested in patients, including a direct comparison to both [^{18}F]NaF and [^{99m}Tc]Tc-MDP.[5,28] Thus, it is a leading candidate for gallium-68 labelled BPs, and hence it was chosen as a BP standard against which [^{68}Ga]Ga-THP-Pam could be compared. [^{18}F]NaF, due to the widespread use and its comparable results to [^{68}Ga]Ga-NO2AP^{BP} in patients with bone metastases,[5] was also included in our comparative *in vivo* study.

The *in vivo* PET-CT imaging results are shown in Figures 6 and 7. All radiotracers were injected intravenously and imaged dynamically for 60 min, showing fast PK profiles and high binding to bone, as expected. The main differences were related to kidney clearance and excretion. Both ^{68}Ga-BPs showed fast renal excretion, but [^{68}Ga]Ga-NO2AP^{BP} cleared faster from the kidneys than [^{68}Ga]Ga-THP-Pam, as demonstrated in Figure 7 by the visible kidney uptake at 40–59 min for [^{68}Ga]Ga-THP-Pam, which was barely visible after 20–40 min in the case of [^{68}Ga]Ga-NO2AP^{BP}. Interestingly, we found a lack of renal clearance with [^{18}F]NaF (Figure 6A). This was surprising as [^{18}F]NaF renal clearance/bladder accumulation is commonly observed in rodent studies, as well as in human clinical PET scans.[5,33] We believe this to be an experimental artefact due to the use of isoflurane anaesthesia, but this hypothesis was not evaluated further. PK data were generated from regions of interest (ROI) within the PET images to calculate the fractions of injected dose per volume (mL) of tissue (Figure 6A). Using the knees as areas with known metabolically active new bone formation, the ROI image-analysis data showed a similar level of binding for both [^{68}Ga]Ga-THP-Pam (14.9 ± 1.0 %ID mL^{-1} at 60 min) and [^{68}Ga]Ga-NO2AP^{BP} (15.7 ± 2.1 %ID mL^{-1} at 60 min) (Figure 6B). Each plateaued at approximately 20 minutes post-injection. In the case of the animals injected with [^{18}F]NaF, knee uptake increased continuously 55 min post-injection, reaching 54.5 ± 5.1 % ID mL^{-1} after 1 h. This significantly higher knee binding of fluoride *vs.* BPs found may be attributable to the lack of excretion discussed above. To determine blood clearance, we used a ROI over the heart as a proxy and the data were fitted to a two-compartment PK model (Figure 6C). All radiotracers showed a two-stage blood clearance with a remarkably similar fast first half life ($t_{1/2}$(fast) = 1.33 ± 0.12 min; mean ± SD for all three radiotracers), followed by a slower clearance stage ($t_{1/2}$(slow) <12 min for all tracers), with the fastest being [^{68}Ga]Ga-NO2AP^{BP} ($t_{1/2}$(slow) = 6.6 min). Accordingly, the area under the curve from 3–59 min ($AUC_{3–59}$) for

[^{68}Ga]Ga-NO2AP^{BP} (98.6 ± 3.4 %ID min mL^{-1}) was lower than that of [^{68}Ga]Ga-THP-Pam (126.4 ± 7.5 %ID min mL^{-1}), and [^{18}F]NaF (122.3 ± 5.1 %ID min mL^{-1}). Thus, whilst both ^{68}Ga-BPs show comparable high bone uptake and fast PK profiles, [^{68}Ga]Ga-NO2AP^{BP} shows slightly faster circulation/renal clearance compared to [^{68}Ga]Ga-THP-Pam.

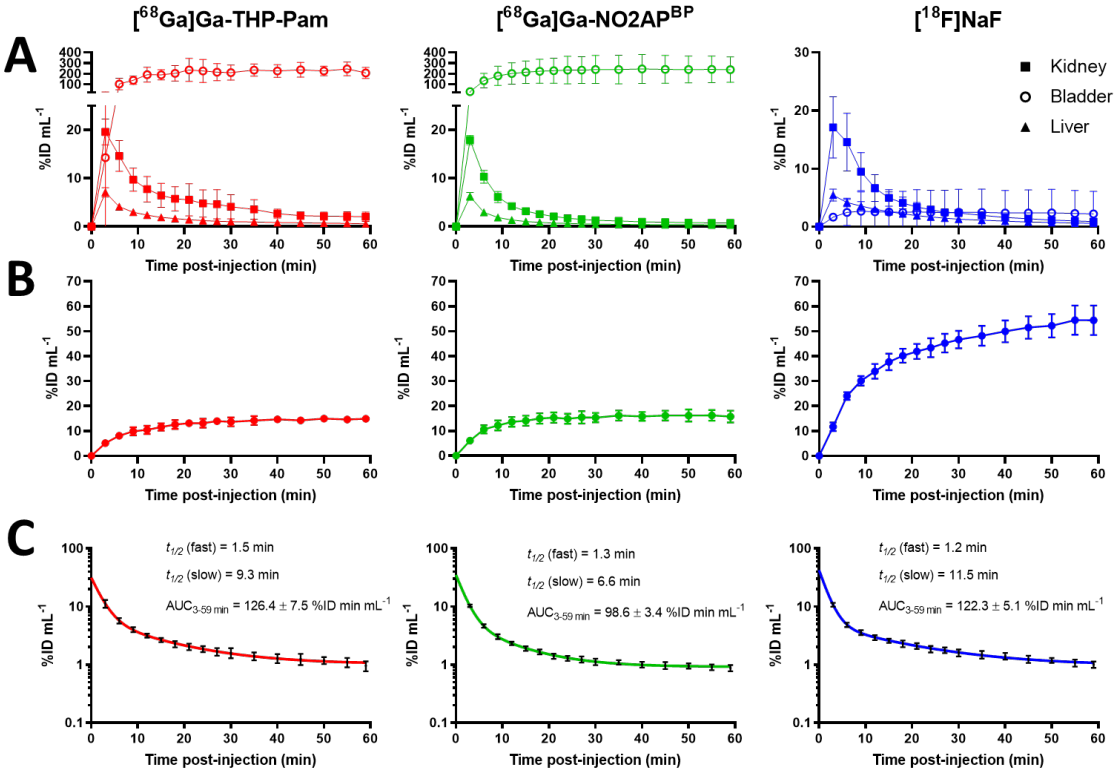

Figure 6. Pharmacokinetic data for the three PET tracers evaluated *in vivo* (n = 4 for each tracer). (A) Activity (%ID/mL) over time (min) in selected organs of interest. (B) Tracer uptake in knee, used as a representative ROI of active bone. (C) Blood clearance fitted to two-compartment pharmacokinetic model using the heart as a representative ROI for blood.

At the end of the imaging session mice were allowed to recover from anaesthesia for 1 h to allow for further radiotracer clearance, and subsequently culled for *ex vivo* biodistribution studies using gamma-counting (Figure 8; values are tabulated in Table S4). Despite the time lag of one hour, the *in vivo* PET imaging analyses results were in agreement with the *ex vivo* biodistribution, with [^{68}Ga]Ga-THP-Pam and [^{68}Ga]Ga-NO2AP^{BP} showing similarly high femur uptake values (14.1 ± 3.7 %ID/g *vs.* 20.1 ± 5.2 % ID/g respectively; p = 0.101) and [^{18}F]NaF having the highest of the three (47.1 ± 8.3 % ID/g) (Figure 8). [^{68}Ga]Ga-THP-Pam showed higher accumulation in kidney and small intestines ($p < 0.001$), although these uptake values were very low (1.4–2.5 % ID/g). These levels of kidney uptake are unlikely to interfere with the imaging of bone metastases or vascular calcification but may be problematic for

imaging calcification in this organ. The bone-to-muscle ratios were similarly high (*ca.* 40) for all three radiotracers (Figure 8).

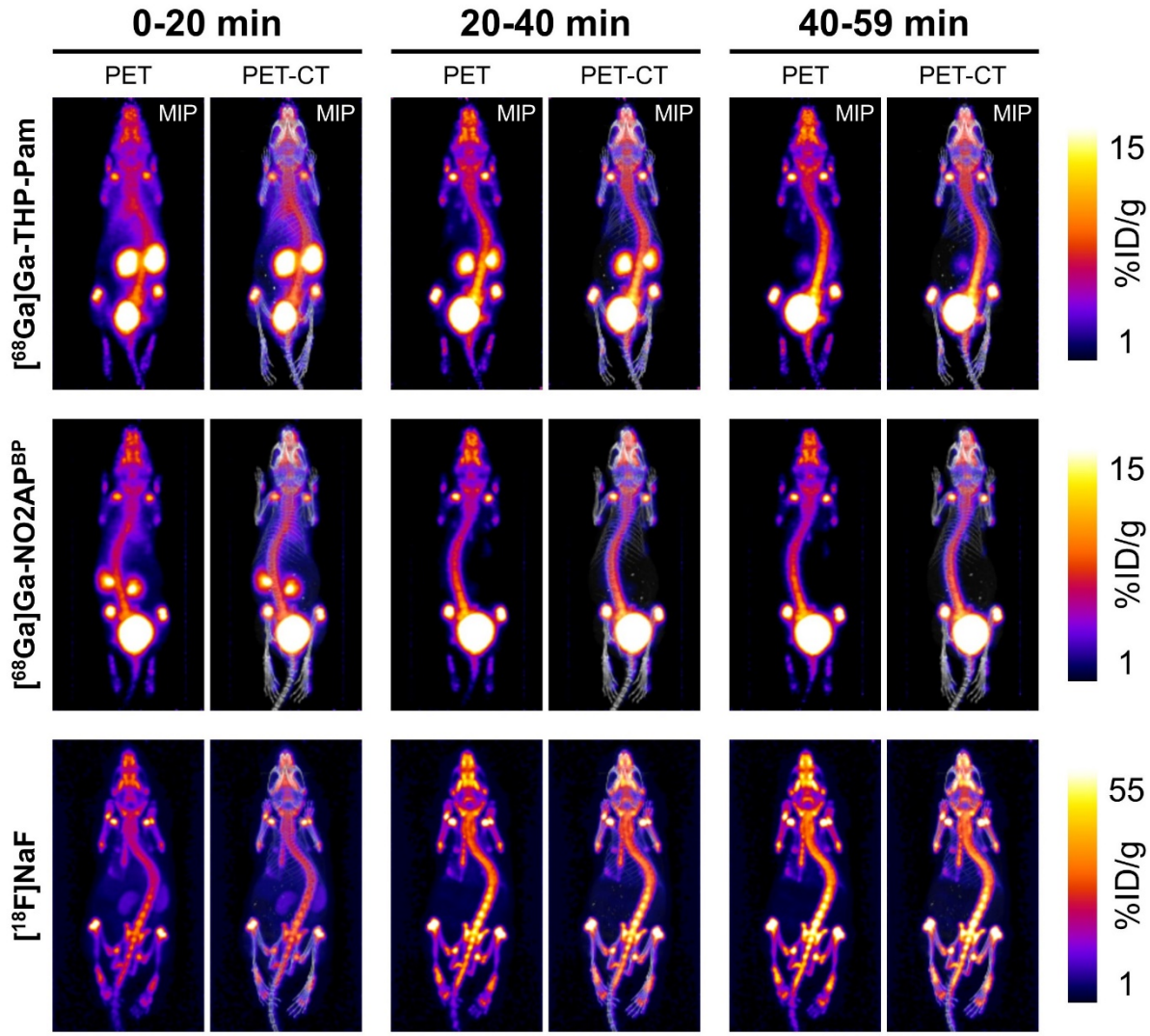

Figure 7. PET-CT study showing representative maximum intensity projection (MIP) images of each radiotracer over three windows of time in healthy BALB/c mice.

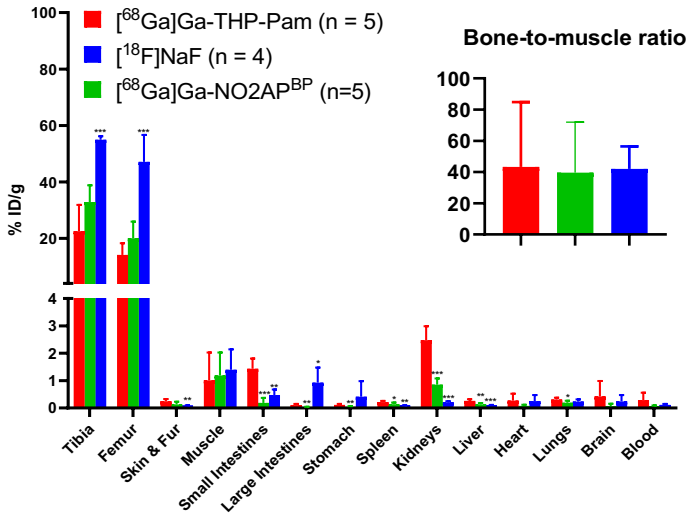

Figure 8. *Ex vivo* biodistribution of [^{68}Ga]Ga-THP-Pam, [^{68}Ga]Ga-NO2AP^{BP} and [^{18}F]NaF 120 min post-injection. Bone-to-muscle ratio inset. * = $p < 0.05$; ** = $p < 0.01$; *** = $p < 0.001$.

Conclusions

[^{68}Ga]Ga-THP-Pam, a new calcium-mineral targeted radiotracer has been synthesised, characterised and evaluated *in vitro* and *in vivo*. Using NMR studies, we demonstrate that gallium binds THP-Pam *via* the THP chelator, and not the bisphosphonate moiety. The THP chelator allows high specific activity ^{68}Ga radiopharmaceuticals with high radiochemical purities (>95%) at room temperature and within minutes. These properties avoid the need for expensive/complicated instrumentation that is common in PET chemistry and allow simple and efficient kit-based radiosynthesis in any radiopharmacy. *In vitro* studies demonstrate that, in contrast to [^{18}F]NaF which is selective to hydroxyapatite, ^{68}Ga-bisphosphonates have high binding affinity to several calcium salts that are present in human calcified vessels, including hydroxyapatite, with the binding of [^{68}Ga]Ga-THP-Pam generally found to be between those of [^{68}Ga]Ga-BPAMD and [^{68}Ga]Ga-NO2AP^{BP}. *In vivo* studies in healthy mice showed that both [^{68}Ga]Ga-THP-Pam and [^{68}Ga]Ga-NO2AP^{BP} (which has been succesfully evaluated in humans, in comparison with [^{18}F]NaF) have a comparable high and rapid uptake in bone tissue, as well as fast blood clearance and urinary excretion. All these results highlight the potential of ^{68}Ga-bisphosphonates as cyclotron-independent alternatives to [^{18}F]NaF, as well as for the imaging of vascular calcification lesions. In addition, the fast, simple and efficient

radiochemistry required to synthesise [^{68}Ga]Ga-THP-Pam makes this radiotracer an appealing candidate for clinical translation.

Materials and Methods

Nomenclature of radiochemical species has been written in accordance with the conventions outlined by Coenen *et al*.[72]

Materials

THP-NCS was obtained from CheMatech, France. All other reagents were purchased from commercial sources unless stated otherwise. NO2AP^{BP} was synthesised according to reference 32. BPAMD was synthesised according to reference 58. Gallium-68 was eluted as [^{68}Ga]$GaCl_3$ from an Eckert & Ziegler ^{68}Ge/^{68}Ga generator in ultra-pure HCl (5 mL, 0.1 M) manufactured to GMP requirements (ABX, Germany). [^{18}F]NaF in H_2O was purchased from Alliance Medical, U.K. ^{1}H and ^{31}P{^{1}H} NMR data were acquired on a Bruker 400 MHz and analysed using MestReNova software. HPLC was performed on an Agilent 1260 Infinity instrument with UV spectroscopic detection at 254 nm and Lablogic Flow-Count detector with Bioscan Inc. B-FC-3200 photomultiplier tube detector and analysed using Laura software. The mobile phase used for analytical and semi-preparative reverse-phase HPLC was composed of A: water with 0.1% TFA and B: MeCN with 0.1% TFA. The mobile phase used for size-exclusion HPLC was PBS. LC/MS data were acquired on an Agilent 1200 Series Liquid Chromatograph with UV spectroscopic detection at 254 nm and same column details as in reverse-phase HPLC, interfaced with an Advion Expression^{L} CMS mass spectrometer with electrospray ionisation source. The mobile phase used for LC/MS was composed of A: water with 0.1% formic acid; and B: MeCN with 0.1% formic acid. Cartridge purification was performed using Sep-Pak tC18 Long Cartridges with 900 mg sorbent per cartridge with a particle size of 37–55 μm. Radio instant thin layer chromatography (ITLC) was developed on Agilent Technologies glass microfibre chromatography paper impregnated with silicic acid and analysed using a Lablogic Flow-count TLC scanner and a BioScan B-FC-3200 PMT detector using Laura software. The ITLC mobile phase was composed of 0.175 M citric acid and 0.325 M trisodium citrate in water unless stated otherwise. Radioactive samples were measured using a Capintec CRC-25R or an LKB Wallac 1282 Compugamma CS for which data were collected using EdenTerm software. PET/CT images were acquired using a NanoPET/CT scanner (Mediso Ltd.,

Budapest, Hungary), reconstructed using Nucline v.0.21 software and images were analysed using VivoQuant® software (version 3.5, InviCRO Inc.). The centrifuge used was a Hettich MIKRO 20. Lyophilisation was performed using an Edwards Freeze Dryer Modulyo.

Synthesis of disodium pamidronate (Pam)

3-aminopropionic acid (15 g, 0.168 mol) and phosphorous acid (20.7 g, 0.252 mol) were suspended in sulfolane (54 mL) and heated to 75°C for 30 min. The mixture was allowed to cool to 35°C and phosphorus trichloride (50 mL, 0.569 mol) was added gradually in aliquots. The solution was heated to 65°C for 3 h with stirring and white precipitate began to form. The suspension was cooled to 0°C and quenched by the slow addition of ice-cold water over 1 h to give a clear solution. The solution was heated to 100°C for 3 h and then cooled to room temperature. Pamidronic acid was precipitated by the addition of ethanol, followed by filtration. The pamidronic acid was suspended in water (100 mL) and aqueous sodium hydroxide (20% w/w) was added with stirring until pH 8 was reached. The mixture was stirred at room temperature for 4 h. The solvents were evaporated and the residue was recrystallized from water/ethanol to give pamidronate disodium dihydrate as a white powder (12.55 g, 39.8 mmol, 24%). ESI-MS: $[M + H]^+$ *m/z* = 235.0; calc. for $C_3H_{12}NO_7P_2$ = 235.0. ^{1}H NMR (D_2O, 400 MHz): δ 3.00–2.90 (2H. t), 2.00–1.88 (2H, m). ^{31}P NMR (D_2O, 162 MHz): δ 17.28. HPLC: 254 nm, t_R = 1.7 min, >99% purity (HPLC method 2). Elemental analysis for disodium pamidronate + 2 H_2O: C = 11.84, H = 4.37, N = 4.45; calc.: C = 11.44, H = 4.16, N = 4.45.

Synthesis of THP-Pam

Pamidronate (14.5 mg, 52 μmol) was dissolved in a mixture of chelex-treated water (200 μL) and triethylamine (21.2 μL, 15.4 mg, 0.15 mmol) and heated to 90°C. Separately, THP-NCS (5 mg, 5.2 μmol) was added to triethylamine (21.2 μL, 15.4 mg, 0.15 mmol) immediately followed by the addition of chelex-treated water (200 μL), and agitated to dissolve the THP-NCS. As soon as the THP-NCS had completely dissolved, the THP-NCS solution was added to the pamidronate solution and stirred in a sealed vial at 90°C for 2 h. The crude mixture was loaded onto a pre-washed Sep-Pak tC18 cartridge and the excess pamidronate was eluted in 5 mL water + 0.1% TFA. The product was eluted in 5 mL 50% water + 0.1% TFA/50% acetonitrile + 0.1% TFA and collected in 0.5 mL fractions. Fractions were analysed by LCMS

and the relevant fractions were combined and lyophilised to yield a white powder (4.40 mg, 3.68 μmol, 71%). ESI-MS: $[M + 2H]^{2+}$ *m/z* = 598.7; calc. for $C_{48}H_{69}N_{11}O_{17}P_2S_2$ = 598.7. ^{1}H NMR (D_2O, 400 MHz): *δ* 7.30–7.05 (4H. m), 6.30–6.20 (3H, m), 4.48 (7H, s), 3.85–3.60 (6H, m), 3.49 (10H, m), 2.43–2.35 (4H, s), 2.23 (11H, m), 2.17–2.09 (8H, m), 1.95–1.82 (6H, m). ^{31}P NMR (D_2O, 162 MHz): *δ* 17.86. HPLC: 254 nm, t_R = 10.4 min, >99% purity (HPLC method 2).

NMR studies of gallium binding

THP-Pam gallium binding

THP-Pam (2.25 mg, 1.88 μmol) was dissolved in D_2O (600 μL), and sodium carbonate in D_2O (1 M) was added to keep the pH in the range 9 and increase solubility of THP-Pam. ^{1}H and ^{31}P NMR spectra were recorded. Gallium nitrate in D_2O (10 μL, 0.627 μmol, 62.7 mM) was added to the NMR tube and more sodium carbonate was added to maintain a pH of 9 with shaking for 5 min. NMR spectra were recorded. This process was repeated two more times until 1 equivalent of gallium had been added.

Pamidronate gallium binding

Pam (3.05 mg, 10.9 μmol) was dissolved in D_2O (600 μL), and sodium carbonate in D_2O (1 M) was added to keep the pH in the range 9 and increase solubility of THP-Pam. The ^{31}P NMR spectrum was recorded. Gallium nitrate in D_2O (43.67 μL, 2.75 μmol, 62.7 mM) was added to the NMR tube and more sodium carbonate was added to maintain a pH of 9, with shaking for 5 min. The ^{31}P NMR spectrum was recorded. This process was repeated three more times until 1 equivalent of gallium had been added.

Synthesis of [^{68}Ga]Ga-THP-Pam

A 1 mg mL^{-1} aqueous solution of THP-Pam in water was prepared. THP-Pam solution (5 μL, 5 μg, 4.18 nmol) was added to [^{68}Ga]$GaCl_3$ (250 μL, 15–90 MBq). Sodium bicarbonate solution in water (26 μL, 1 M) was added immediately. The mixture was agitated and the pH was checked to ensure it was in the range 6.5–7.5. Radiochemical yield and purity were evaluated after 5 min by ITLC (unbound ^{68}Ga R_f = 0.8–1; [^{68}Ga]Ga-THP-Pam R_f = 0–0.3) and after 10 min by HPLC, method 2 (unbound ^{68}Ga t_R = 1.9 min; [^{68}Ga]Ga-THP-Pam t_R = 10.8 min).

Synthesis of [^{68}Ga]Ga-NO2AP^{BP}

Gallum-68 (140–200 MBq) eluted from a generator was passed through a Phenomenex Strata-X-C 33 μm SPE cartridge. The cartridge was washed with acetone/0.1 M hydrochloric acid (80:20 v/v, 5 mL) to remove trace metal impurities. The gallium-68 was recovered from the cartridge by washing slowly with acetone/0.05 M hydrochloric acid (98/2 v/v, 700 μL) and added to aqueous HEPES buffer (pH 4, 0.125 M, 400 μL). Aqueous 1 mg mL^{-1} NO2AP^{BP} (8.69 μL, 8.69 μg, 17 nmol) was added to the gallium-68/HEPES solution followed by heating to 95°C for 10 min with venting to allow the acetone to evaporate. After cooling, pH was adjusted to 7 by adding aqueous sodium hydroxide (~10 μL, 1 M).

Determination of LogP and Log $D_{7.4}$ values

For logP measurement, aliquots of [^{68}Ga]Ga-THP-Pam (10 μL, ~700 kBq) were added to vials containing a mixture of octanol pre-saturated with water (500 μL) and water pre-saturated with octanol (500 μL). The tubes were shaken for 3 min and the mixture was centrifuged for 5 min to separate the octanol and PBS phases. Aliquots (50 μL) of each phase were taken and transferred to separate vials for counting of radioactivity. For measurement of log$D_{7.4}$ the same procedure was performed, using PBS in place of water.

Serum stability

Freshly filtered human serum (200 μL) was added to a tube containing normal saline (100 μL) followed by incubation at 37°C. [^{68}Ga]Ga-THP-Pam (100 μL, ~7 MBq) was added. Size exclusion HPLC (using method 3 (Table S3) was run prior to incubation, and after 60 and 180 min of incubation. Serum proteins eluted at 5.0–9.0 min. [^{68}Ga]Ga-THP-Pam eluted at 11.0 min.

Stability to EDTA competition

An aliquot of EDTA solution in PBS (950 μL, 1 mM) was incubated at 37°C. [^{68}Ga]Ga-THP-Pam (50 μL, ~20 MBq) was added to the EDTA solution and incubated with stirring. Samples were analysed by ITLC (mobile phase: 1 M ammonium acetate in 1:1 water/methanol) after 60 min and 180 min. Controls were performed using [^{68}Ga]$GaCl_3$ neutralised according to the method used in the synthesis of [^{68}Ga]Ga-THP-Pam, in the absence of the THP-Pam ligand. Unbound ^{68}Ga R_f = 0–0.3; [^{68}Ga]Ga-THP-Pam R_f = 0–0.3; [^{68}Ga]Ga-EDTA R_f = 0.7–1.

Binding to calcium salts

A suspension of HAp (1 mg) in saline (1 mL) was prepared. For the blocking study this was prepared in advance with pamidronate (27.9 mg, 100 μmol) and incubated overnight prior to reaction. Once the suspensions were prepared, an aliquot of the reaction mixture containing the radiotracer (10 μL, ~700 kBq) was added to the suspension and incubated at room temperature for 1 h with continuous shaking. The suspensions were centrifuged at 9677 g for 5 min and the supernatant was removed to a new tube and the activities of both fractions were measured. All the above steps were also repeated with other calcium salts (CC, CP dibasic, CPy, β-TCP, CO). These measurements were repeated for [^{68}Ga]Ga-BPAMD (blocking with alendronate), [^{68}Ga]Ga-NO2AP^{BP} (blocking with pamidronate) and [^{18}F]NaF (blocking with sodium fluoride).

PET-CT imaging

Animal imaging studies were ethically reviewed and carried out in accordance with the Animals (Scientific Procedures) Act 1986 (ASPA) U.K. Home Office regulations governing animal experimentation. Each mouse (5 per tracer, of which 4 were imaged and 1 was used only for biodistribution studies, normal BALB/c, female, aged 6–8 weeks, 17–20 g body weight) was anaesthetised by inhalation of isoflurane (2–3% in oxygen), the tail vein was cannulated. Then the mouse was placed in a preclinical PET/CT scanner, where anaesthesia was maintained and the bed was heated to maintain normal body temperature. CT was performed followed by 1 hour PET acquisition (1:5 coincidence mode; 5-ns coincidence time window). After the first minute, the radiopharmaceutical (100 ± 15 μL, 2.2–16.2 MBq) was injected and the animal was scanned. At the end of the scan, the animal was removed and allowed to recover for a further hour and culled at 2 h post-injection for biodistribution studies. Organs were harvested, weighed and counted with a gamma counter along with standards prepared from injected material. Dynamic PET/CT images were reconstructed using Tera-Tomo 3D reconstruction (400–600 keV energy window, 1–3 coincidence mode, 4 iterations and subsets) at a voxel size of (0.4 × 0.4 × 0.4) mm^3 and corrected for attenuation, scatter and decay. The data were binned into 17 frames (1 × 1, 10 × 3, 5 × 5 and 1 × 4 min) for dynamic analysis. Regions of interest were drawn over the knees as an area of growing bone, heart as an indication of blood, kidneys, bladder and liver.

Acknowledgements

The authors would like to thank A. Mishra, A. Khan, J. Jackson, and P. Gawne for their assistance during the *in vivo* work and D. Thakor, M. Hutchings, K. Sunassee and S. Catchpole for their technical support. Elemental analyses were performed by Stephen Young, Chief Research Technician, Microanalysis, Department of Chemistry, University of Cambridge. This work was funded by the EPSRC Centre for Doctoral Training in Medical Imaging [EP/L015226/1], Theragnostics Ltd., the Wellcome/EPSRC Centre for Medical Engineering [WT/203148/Z/16/Z], and the EPSRC programme for next generation molecular imaging and therapy with radionuclides [EP/S032789/1]. Further support comes from a Wellcome Trust Multi User Equipment Grant: A multiuser radioanalytical facility for molecular imaging and radionuclide therapy research and the National Institute for Health Research (NIHR) Biomedical Research Centre based at Guy's and St Thomas' NHS Foundation Trust and KCL [grant number IS-BRC-1215-20006]. PET and SPECT scanning equipment at KCL was funded by an equipment grant from the Wellcome Trust under grant number WT 084052/Z/07/Z. The views expressed are those of the authors and not necessarily those of the NHS, the NIHR or the Department of Health.

Supporting Information

Supporting information. HPLC and LC/MS methods, biodistribution data, stability in EDTA data.

References

(1) Peacock, M. (2010) Calcium Metabolism in Health and Disease. *Clin. J. Am. Soc. Nephrol. 5*, S23-S30.

(2) Lippard, S. J., and Berg, J. M. (1994) *Principles of bioinorganic chemistry*, Mill Valley, California: University Science Books, Mill Valley, California.

(3) Clarke, B. (2008) Normal bone anatomy and physiology. *Clin. J. Am. Soc. Nephrol. 3* S131-S139.

(4) O'Sullivan, G. J., Carty, F. L., and Cronin, C. G. (2015) Imaging of bone metastasis: An update. *World J. Radiol. 7*, 202-211.

(5) Pfannkuchen, N., Meckel, M., Bergmann, R., Bachmann, M., Bal, C., Sathekge, M., Mohnike, W., Baum, R., and Rösch, F. (2017) Novel Radiolabeled Bisphosphonates for PET Diagnosis and Endoradiotherapy of Bone Metastases. *Pharmaceuticals 10*, 45.

(6) Qiu, L., Lin, J. G., Ju, X. H., Gong, X. D., and Luo, S. N. (2011) Structural Investigation of Technetium-Diphosphonate Complex Tc-99m-MDP. *Chin. J. Chem. Phys. 24*, 295-304.

(7) Subramanian, G., McAfee, J. G., Blair, R. J., Kallfelz, F. A., and Thomas, F. D. (1975) Technetium 99m methylene diphosphonate: a superior agent for skeletal imaging: Comparison with other technetium complexes. *J. Nucl. Med. 16*, 744-755.

(8) Handeland, A., Lindegaard, M. W., and Heggli, D. E. (1989) Biodistribution of anionic separated MDP complexes from different MDP preparations. *Eur. J. Nucl. Med. 15*, 609-611.

(9) Hillner, B. E., Siegel, B. A., Hanna, L., Duan, F., Quinn, B., and Shields, A. F. (2015) 18F-Fluoride PET Used for Treatment Monitoring of Systemic Cancer Therapy: Results from the National Oncologic PET Registry. *J. Nucl. Med. 56*, 222-228.

(10) Beheshti, M., Mottaghy, F. M., Payche, F., Behrendt, F. F. F., Van den Wyngaert, T., Fogelman, I., Strobel, K., Celli, M., Fanti, S., Giammarile, F.; et al. (2015) 18F-NaF PET/CT: EANM procedure guidelines for bone imaging. *Eur. J. Nucl. Med. Mol. Imag. 42*, 1767-1777.

(11) Segall, G., Delbeke, D., Stabin, M. G., Even-Sapir, E., Fair, J., Sajdak, R., and Smith, G. T. (2010) SNM Practice Guideline for Sodium 18F-Fluoride PET/CT Bone Scans 1.0. *J. Nucl. Med. 51*, 1813-1820.

(12) Czernin, J., Satyamurthy, N., and Schiepers, C. (2010) Molecular Mechanisms of Bone 18F-NaF Deposition. *J. Nucl. Med. 51*, 1826-1829.

(13) Doherty, T. M., Asotra, K., Fitzpatrick, L. A., Qiao, J.-H., Wilkin, D. J., Detrano, R. C., Dunstan, C. R., Shah, P. K., and Rajavashisth, T. B. (2003) Calcification in atherosclerosis: Bone biology and chronic inflammation at the arterial crossroads. *Proc. Natl. Acad. Sci. U. S. A. 100*, 11201-11206.

(14) Virani, S. S., Alonso, A., Benjamin, E. J., Bittencourt, M. S., Callaway, C. W., Carson, A. P., Chamberlain, A. M., Chang, A. R., Cheng, S., Delling, F. N.; et al. (2020) Heart Disease and Stroke Statistics-2020 Update: A Report From the American Heart Association. *Circulation 141*, e139-e596.

(15) Nishizawa, Y., Higuchi, C., Nakaoka, T., Omori, H., Ogawa, T., Sakura, H., and Nitta, K. (2018) Compositional Analysis of Coronary Artery Calcification in Dialysis Patients in vivo by Dual-Energy Computed Tomography Angiography. *Theor. Apheresis Dial. 22*, 365-370.

(16) Schwarz, U., Buzello, M., Ritz, E., Stein, G., Raabe, G., Wiest, G., Mall, G., and Amann, K. (2000) Morphology of coronary atherosclerotic lesions in patients with end-stage renal failure. *Nephrol. Dial. Transplant. 15*, 218-23.

(17) Schlieper, G., Aretz, A., Verberckmoes, S. C., Krüger, T., Behets, G. J., Ghadimi, R., Weirich, T. E., Rohrmann, D., Langer, S., Tordoir, J. H.; et al. (2010) Ultrastructural analysis of vascular calcifications in uremia. *J. Am. Soc. Nephrol. 21*, 689-696.

(18) O'Neill, W. C. (2007) Vascular calcification: Not so crystal clear. *Kidney Int. 71*, 282-283.

(19) Villa-Bellosta, R., and Egido, J. (2015) Phosphate, pyrophosphate, and vascular calcification: a question of balance. *Eur. Heart J. 38*, 1801-1804.

(20) Reid, J. D., and Andersen, M. E. (1993) Medial calcification (whitlockite) in the aorta. *Atherosclerosis 101*, 213-24.

(21) Lee, J. S., Morrisett, J. D., and Tung, C.-H. (2012) Detection of hydroxyapatite in calcified cardiovascular tissues. *Atherosclerosis 224*, 340-347.

(22) Creager, M. D., Hohl, T., Hutcheson, J. D., Moss, A. J., Schlotter, F., Blaser, M. C., Park, M.-A., Lee, L. H., Singh, S. A., Alcaide-Corral, C. J.; et al. (2019) 18F-Fluoride Signal Amplification Identifies Microcalcifications Associated With Atherosclerotic Plaque Instability in Positron Emission Tomography/Computed Tomography Images. *Circ. Cardiovasc. Imaging 12*, e007835.

(23) Irkle, A., Vesey, A. T., Lewis, D. Y., Skepper, J. N., Bird, J. L. E., Dweck, M. R., Joshi, F. R., Gallagher, F. A., Warburton, E. A., Bennett, M. R.; et al. (2015) Identifying active vascular microcalcification by F-18-sodium fluoride positron emission tomography. *Nat. Commun. 6*, 11.

(24) de Rosales, R. T. M., Finucane, C., Mather, S. J., and Blower, P. J. (2009) Bifunctional bisphosphonate complexes for the diagnosis and therapy of bone metastases. *Chem. Commun.*, 4847-4849.

(25) de Rosales, R. T. M., Tavare, R., Paul, R. L., Jauregui-Osoro, M., Protti, A., Glaria, A., Varma, G., Szanda, I., and Blower, P. J. (2011) Synthesis of Cu-64(II)-Bis(dithiocarbamatebisphosphonate) and Its Conjugation with Superparamagnetic Iron Oxide Nanoparticles: In Vivo Evaluation as Dual-Modality PET-MRI Agent. *Angew. Chem. Int. Ed. 50*, 5509-5513.

(26) Fellner, M., Baum, R. P., Kubicek, V., Hermann, P., Lukes, I., Prasad, V., and Rosch, F. (2010) PET/CT imaging of osteoblastic bone metastases with Ga-68-bisphosphonates: first human study. *Eur. J. Nucl. Med. Mol. Imag. 37*, 834-834.

(27) Khawar, A., Eppard, E., Roesch, F., Ahmadzadehfar, H., Kurpig, S., Meisenheimer, M., Gaertner, F. C., Essler, M., and Bundschuh, R. A. (2019) Preliminary results of biodistribution and dosimetric analysis of Ga-68 Ga-DOTA(ZOL): a new zoledronate-based bisphosphonate for PET/CT diagnosis of bone diseases. *Ann. Nucl. Med. 33*, 404-413.

(28) Passah, A., Tripathi, M., Ballal, S., Yadav, M. P., Kumar, R., Roesch, F., Meckel, M., Sarathi Chakraborty, P., and Bal, C. (2017) Evaluation of bone-seeking novel radiotracer 68Ga-NO2AP-Bisphosphonate for the detection of skeletal metastases in carcinoma breast. *Eur. J. Nucl. Med. Mol. Imag. 44*, 41-49.

(29) Doot, R. K., Young, A. J., Daube-Witherspoon, M. E., Alexoff, D., Labban, K. J., Lee, H., Wu, Z., Zha, Z., Choi, S. R., Ploessl, K. H.; et al. (2020) Biodistribution, dosimetry, and temporal signal-to-noise ratio analyses of normal and cancer uptake of [68Ga]Ga-P15-041, a gallium-68 labeled bisphosphonate, from first-in-human studies. *Nucl. Med. Biol. 86-87*, 1-8.

(30) Lawal, I. O., Mokoala, K. M. G., Mahapane, J., Kleyhans, J., Meckel, M., Vorster, M., Ebenhan, T., Rosch, F., and Sathekge, M. M. (2020) A prospective intra-individual comparison of Ga-68 Ga-PSMA-11 PET/CT, Ga-68 Ga-NODAGA(ZOL) PET/CT, and Tc-99m Tc-MDP bone scintigraphy for radionuclide imaging of prostate cancer skeletal metastases. *Eur. J. Nucl. Med. Mol. Imag.*

(31) Fellner, M., Biesalski, B., Bausbacher, N., Kubicek, V., Hermann, P., Rosch, F., and Thews, O. (2012) Ga-68-BPAMD: PET-imaging of bone metastases with a generator based positron emitter. *Nucl. Med. Biol. 39*, 993-999.

(32) Holub, J., Meckel, M., Kubicek, V., Rosch, F., and Hermann, P. (2015) Gallium(III) complexes of NOTA-bis (phosphonate) conjugates as PET radiotracers for bone imaging. *Contrast Media Mol. Imaging 10*, 122-34.

(33) Meckel, M., Fellner, M., Thieme, N., Bergmann, R., Kubicek, V., and Rosch, F. (2013) In vivo comparison of DOTA based Ga-68-labelled bisphosphonates for bone imaging in non-tumour models. *Nucl. Med. Biol. 40*, 823-830.

(34) Rosch, F., and Baum, R. P. (2011) Generator-based PET radiopharmaceuticals for molecular imaging of tumours: on the way to THERANOSTICS. *Dalton Trans. 40*, 6104-11.

(35) Suzuki, K., Satake, M., Suwada, J., Oshikiri, S., Ashino, H., Dozono, H., Hino, A., Kasahara, H., and Minamizawa, T. (2011) Synthesis and evaluation of a novel Ga-68-chelate-conjugated bisphosphonate as a bone-seeking agent for PET imaging. *Nucl. Med. Biol. 38*, 1011-1018.

(36) Notni, J., Plutnar, J., and Wester, H. J. (2012) Bone-seeking TRAP conjugates: surprising observations and their implications on the development of gallium-68-labeled bisphosphonates. *EJNMMI Res. 2*.

(37) Wu, Z., Zha, Z., Choi, S. R., Plossl, K., Zhu, L., and Kung, H. F. (2016) New (68)Ga-PhenA bisphosphonates as potential bone imaging agents. *Nucl. Med. Biol. 43*, 360-71.

(38) Meckel, M., Bergmann, R., Miederer, M., and Roesch, F. (2016) Bone targeting compounds for radiotherapy and imaging: *Me(III)-DOTA conjugates of bisphosphonic acid, pamidronic acid and zoledronic acid. *EJNMMI Radiopharm. Chem. 1*, 14.

(39) Ahrens, B. J., Li, L., Ciminera, A. K., Chea, J., Poku, E., Bading, J. R., Weist, M. R., Miller, M. M., Colcher, D. M., and Shively, J. E. (2017) Diagnostic PET Imaging of Mammary Microcalcifications Using Cu-64-DOTA-Alendronate in a Rat Model of Breast Cancer. *J. Nucl. Med. 58*, 1373-1379.

(40) Zha, Z., Wu, Z., Choi, S. R., Ploessl, K., Smith, M., Alexoff, D., Zhu, L., and Kung, H. F. (2020) A New [68Ga]Ga-HBED-CC-Bisphosphonate as a Bone Imaging Agent. *Mol. Pharm. 17*, 1674-1684.

(41) Fani, M., Andre, J. P., and Maecke, H. R. (2008) 68Ga-PET: a powerful generator-based alternative to cyclotron-based PET radiopharmaceuticals. *Contrast Media Mol. Imaging 3*, 67-77.

(42) Banerjee, S. R., Pullambhatla, M., Byun, Y., Nimmagadda, S., Green, G., Fox, J. J., Horti, A., Mease, R. C., and Pomper, M. G. (2010) 68Ga-Labeled Inhibitors of Prostate-Specific Membrane Antigen (PSMA) for Imaging Prostate Cancer. *J. Med. Chem. 53*, 5333-5341.

(43) Eder, M., Schäfer, M., Bauder-Wüst, U., Hull, W.-E., Wängler, C., Mier, W., Haberkorn, U., and Eisenhut, M. (2012) 68Ga-Complex Lipophilicity and the Targeting Property of a Urea-Based PSMA Inhibitor for PET Imaging. *Bioconjugate Chem. 23*, 688-697.

(44) Young, J. D., Abbate, V., Imberti, C., Meszaros, L. K., Ma, M. T., Terry, S. Y. A., Hider, R. C., Mullen, G. E., and Blower, P. J. (2017) Ga-68-THP-PSMA: A PET Imaging Agent for Prostate Cancer Offering Rapid, Room-Temperature, 1-Step Kit-Based Radiolabeling. *J. Nucl. Med. 58*, 1270-1277.

(45) Graham, M. M., Gu, X., Ginader, T., Breheny, P., and Sunderland, J. (2017) 68Ga-DOTATOC Imaging of Neuroendocrine Tumors: A Systematic Review and Meta-Analysis. *J. Nucl. Med.*

(46) Giesel, F. L., Kratochwil, C., Lindner, T., Marschalek, M. M., Loktev, A., Lehnert, W., Debus, J., Jager, D., Flechsig, P., Altmann, A.; et al. (2019) Ga-68-FAPI PET/CT: Biodistribution and Preliminary Dosimetry Estimate of 2 DOTA-Containing FAP-Targeting Agents in Patients with Various Cancers. *J. Nucl. Med. 60*, 386-392.

(47) Ma, M. T., Cullinane, C., Waldeck, K., Roselt, P., Hicks, R. J., and Blower, P. J. (2015) Rapid kit-based (68)Ga-labelling and PET imaging with THP-Tyr(3)-octreotate: a preliminary comparison with DOTA-Tyr(3)-octreotate. *EJNMMI Res. 5*, 52.

(48) Hofman, M. S., Eu, P., Jackson, P., Hong, E., Binns, D., Iravani, A., Murphy, D., Mitchell, C., Siva, S., Hicks, R. J.; et al. (2018) Cold Kit for Prostate-Specific Membrane Antigen (PSMA) PET Imaging: Phase 1 Study of (68)Ga-Tris(Hydroxypyridinone)-PSMA PET/CT in Patients with Prostate Cancer. *J. Nucl. Med. 59*, 625-631.

(49) Berry, D. J., Ma, Y. M., Ballinger, J. R., Tavare, R., Koers, A., Sunassee, K., Zhou, T., Nawaz, S., Mullen, G. E. D., Hider, R. C.; et al. (2011) Efficient bifunctional gallium-68 chelators for positron emission tomography: tris(hydroxypyridinone) ligands. *Chem. Commun. 47*, 7068-7070.

(50) Ma, M. T., Cullinane, C., Imberti, C., Baguna Torres, J., Terry, S. Y. A., Roselt, P., Hicks, R. J., and Blower, P. J. (2016) New Tris(hydroxypyridinone) Bifunctional Chelators Containing Isothiocyanate Groups Provide a Versatile Platform for Rapid One Step Labeling and PET Imaging with Ga-68(3+). *Bioconjugate Chem. 27*, 309-318.

(51) Imberti, C., Terry, S. Y. A., Cullinane, C., Clarke, F., Cornish, G. H., Ramakrishnan, N. K., Roselt, P., Cope, A. P., Hicks, R. J., Blower, P. J.; et al. (2017) Enhancing PET Signal at Target Tissue in Vivo: Dendritic and Multimeric Tris(hydroxypyridinone) Conjugates for Molecular Imaging of alpha(v)beta(3) Integrin Expression with Gallium-68. *Bioconjugate Chem. 28*, 481-495.

(52) Nawaz, S., Mullen, G. E. D., Sunassee, K., Bordoloi, J., Blower, P. J., and Ballinger, J. R. (2017) Simple, mild, one-step labelling of proteins with gallium-68 using a tris(hydroxypyridinone) bifunctional chelator: a 68Ga-THP-scFv targeting the prostate-specific membrane antigen. *EJNMMI Res. 7*, 86.

(53) Tsionou, M. I., Knapp, C. E., Foley, C. A., Munteanu, C. R., Cakebread, A., Imberti, C., Eykyn, T. R., Young, J. D., Paterson, B. M., Blower, P. J.; et al. (2017) Comparison of macrocyclic and acyclic chelators for gallium-68 radiolabelling. *RSC Adv. 7*, 49586-49599.

(54) Cusnir, R., Cakebread, A., Cooper, M. S., Young, J. D., Blower, P. J., and Ma, M. T. (2019) The effects of trace metal impurities on Ga-68-radiolabelling with a tris(3-hydroxy-1,6-dimethylpyridin-4-one) (THP) chelator. *RSC Adv. 9*, 37214-37221.

(55) Imberti, C., Chen, Y. L., Foley, C. A., Ma, M. T., Paterson, B. M., Wang, Y. F., Young, J. D., Hider, R. C., and Blower, P. J. (2019) Tuning the properties of tris(hydroxypyridinone) ligands: efficient Ga-68 chelators for PET imaging. *Dalton Trans. 48*, 4299-4313.

(56) Imberti, C., Adumeau, P., Blower, J. E., Al Salemee, F., Torres, J. B., Lewis, J. S., Zeglis, B. M., Terry, S. Y. A., and Blower, P. J. (2020) Manipulating the In Vivo Behaviour of Ga-68 with Tris(Hydroxypyridinone) Chelators: Pretargeting and Blood Clearance. *Int. J. Mol. Sci. 21*, 19.

(57) Cusnir, R., Imberti, C., Hider, R. C., Blower, P. J., and Ma, M. T. (2017) Hydroxypyridinone Chelators: From Iron Scavenging to Radiopharmaceuticals for PET Imaging with Gallium-68. *Int. J. Mol. Sci. 18*, 1-23.

(58) Kubicek, V., Rudovsky, J., Kotek, J., Hermann, P., Elst, L. V., Muller, R. N., Kolar, Z. I., Wolterbeek, H. T., Peters, J. A., and Lukes, I. (2005) A bisphosphonate monoamide analogue of DOTA: A potential agent for bone targeting. *J. Am. Chem. Soc. 127*, 16477-16485.

(59) Fitton, A., and McTavish, D. (1991) Pamidronate. A review of its pharmacological properties and therapeutic efficacy in resorptive bone disease. *Drugs 41*, 289-318.

(60) Patel, V. M., Chitturi, T. R., and Thennati, R. (2008), Google Patents.

(61) Saari, A.-L., Hyvönen, H., Lahtinen, M., Ylisirniö, M., Turhanen, P., Kolehmainen, E., Peräniemi, S., and Vepsäläinen, J. (2012) Systematic study of the physicochemical properties of a homologous series of aminobisphosphonates. *Molecules (Basel, Switzerland) 17*, 10928-10945.

(62) Algar, W. R. (2018) A Brief Introduction to Traditional Bioconjugate Chemistry, in *Chemoselective and Bioorthogonal Ligation Reactions: Concepts and Application* (Algar, W. R., Dawson, P. E., and Medintz, I. L., Eds.) pp 3-36, Wiley-VCH, Weinheim, Germany.

(63) Banks, P. R., and Paquette, D. M. (1995) Comparison of Three Common Amine Reactive Fluorescent Probes Used for Conjugation to Biomolecules by Capillary Zone Electrophoresis. *Bioconjugate Chem. 6*, 447-458.

(64) Landel, A. M. (1976) Stability studies on fluorescein isothiocyanate-bovine serum albumin conjugate. *Anal. Biochem. 73*, 280-289.

(65) Fleisch, H. (1998) Bisphosphonates: Mechanisms of Action. *Endocr. Rev. 19*, 80-100.

(66) T. M. de Rosales, R., Tavare, R., Glaria, A., Varma, G., Protti, A., and Blower, P. J. (2011) Tc-99m-Bisphosphonate-Iron Oxide Nanoparticle Conjugates for Dual-Modality Biomedical Imaging. *Bioconjugate Chem. 22*, 455-465.

(67) Sandiford, L., Phinikaridou, A., Protti, A., Meszaros, L. K., Cui, X. J., Yan, Y., Frodsham, G., Williamson, P. A., Gaddum, N., Botnar, R. M.; et al. (2013) Bisphosphonate-Anchored PEGylation and Radiolabeling of Superparamagnetic Iron Oxide: Long-Circulating Nanoparticles for in Vivo Multimodal (T1 MRI-SPECT) Imaging. *ACS Nano 7*, 500-512.

(68) Subramanian, G., and McAfee, J. G. (1971) A new complex of 99mTc for skeletal imaging. *Radiology 99*, 192-6.

(69) Young, J. Imaging and Therapeutic Radiotracers for Prostate Cancer. Ph.D. Thesis, King's College London, London, U.K., 2018

(70) Velikyan, I., Maecke, H., and Langstrom, B. (2008) Convenient Preparation of 68Ga-Based PET-Radiopharmaceuticals at Room Temperature. *Bioconjugate Chem. 19*, 569-573.

(71) Seemann, J., Eppard, E., Waldron, B. P., Ross, T. L., and Roesch, F. (2015) Cation exchange-based post-processing of Ga-68-eluate: A comparison of three solvent systems for labelling of DOTATOC, NO2AP(BP) and DATA(m). *Appl. Radiat. Isot. 98*, 54-59.

(72) Coenen, H. H., Gee, A. D., Adam, M., Antoni, G., Cutler, C. S., Fujibayashi, Y., Jeong, J. M., Mach, R. H., Mindt, T. L., Pike, V. W.; et al. (2017) Consensus nomenclature rules for radiopharmaceutical chemistry — Setting the record straight. *Nucl. Med. Biol. 55*, v-xi.